Chinese Chemical Letters 36 (2025) 110399

Contents lists available at ScienceDirect

Chinese Chemical Letters

journal homepage: www.elsevier.com/locate/cclet

High efficiency conversion of low concentration nitrate boosted with amorphous Cu^0 nanorods prepared *via in-situ* reconstruction

Yunqing Zhu[a,*], Kaiyue Wen[a], Xuequan Wan[a], Gaigai Dong[a], Junfeng Niu[b]

[a] School of Environmental Science and Engineering, Shaanxi University of Science and Technology, Xi'an 710021, China
[b] College of Environmental Science and Engineering, North China Electric Power University, Beijing 102206, China

ARTICLE INFO

Article history:
Received 23 May 2024
Revised 23 July 2024
Accepted 31 August 2024
Available online 1 September 2024

Keywords:
Cu_3N
Electrochemical reconstruction
Cu^0 nanorods
Amorphous structure
Electrochemical nitrate reduction

ABSTRACT

Electrocatalytic nitrate reduction reaction (NO_3^-RR) is a green and competitive method for removing nitrate from water, requiring highly active and long-term stable electrocatalysts. In this work, we report a Cu^0 nanorod catalyst with disordered structure (re-Cu NRs), prepared by electrochemical *in situ* reconfiguration of copper-based nitrides (Cu_3N NRs). The amorphous structure allows the exposure of abundant active sites to enhance the electrocatalytic activity because of the disordered atomic arrangement. At a potential of −1.2 V *vs.* Ag/AgCl, the re-Cu NRs catalyst achieved nearly 100% nitrate conversion within 120 min at a low nitrate concentration (50 mg/L), without the accumulation of nitrite. *In-situ* DEMS detection reveals that the NO_3^-RR on re-Cu NRs followed the pathway of $^*NO_3^- \rightarrow {}^*NO_2^- \rightarrow {}^*NO \rightarrow {}^*N \rightarrow {}^*NH \rightarrow {}^*NH_2 \rightarrow {}^*NH_3$. Furthermore, combining this proposed pathway with electrochlorination could efficiently transform ammonia into harmless N_2 (~99.41%). Theoretical calculations confirm that the amorphous structure on the surface of re-Cu NRs catalysts can facilitate strongly adsorbed nitrate, weaken the rate-determining step of $^*NH_3 \rightarrow NH_3$, and suppress hydrogen evolution reaction (HER). This study provides a new approach for designing efficient and stable amorphous catalysts for electrocatalytic nitrate reduction.

Due to human intervention in the nitrogen cycle, including the widespread use of nitrogen-containing fertilizers and the discharge of domestic or industrial wastewater, nitrate pollution has affected both surface and groundwater [1,2]. Apart from harming aquatic ecosystems, nitrate pollution in water can lead to severe human health issues [3]. In response to this, the World Health Organization (WHO) has set the maximum permissible nitrate concentration in drinking water at 10 mg/L [4]. Some technologies such as biological denitrification, ion exchange, reverse osmosis, and electrodialysis have been developed to remediate nitrate-rich wastewater [5-8]. Nevertheless, they come with inevitable drawbacks, including secondary pollution, slow reaction rates, and high reaction costs, making them unsuitable for large-scale applications [9,10]. In recent years, electrocatalytic nitrate reduction reaction (NO_3^-RR), utilizing electrons as a clean reducing agent to convert nitrate into ammonia or harmless nitrogen gas, has emerged as a promising method for mitigating nitrate pollution [11,12]. However, considering the fact that many practical sources of nitrate wastewater, such as natural/industrial wastewater, have low concentrations ranging from hundreds to thousands of ppm [13,14]. It is crucial for the development of advanced electrocatalysts to enhance nitrate reduction at low initial NO_3^--N concentrations.

To date, various transition metal catalysts, such as Cu, Fe, Ni, and Co, have been studied for their application in the electrochemical reduction of NO_3^--N in water [4,15-18]. Among them, low-cost and non-toxic copper-based catalysts exhibit strong NO_3^--N adsorption capability, especially in the dilute nitrate system, which demonstrates the highest reaction kinetics in the rate-determining step in NO_3^-RR (conversion of NO_3^--N to NO_2^--N) [19]. However, single-component copper-based catalysts suffer from poor catalyst stability and low ammonia selectivity due to competitive adsorption of intermediate products. To address these issues, researchers have proposed various solutions, such as doping, alloy strategies, and the preparation of copper-based oxides, to enhance nitrate reduction [20-22]. Recently, Wang *et al.* [18] discovered that copper-based oxides undergo *in-situ* transformation to Cu^0 during electrochemical reactions, and their performance surpasses that of CuO and Cu_2O. Ren *et al.* [23] developed a multi-phase heterostructure material Cu/Pd/CuO_x through *in-situ* restructuring, exhibiting excellent NO_3^-RR catalytic activity. Under conditions of −1.3 V *vs.* SCE, ammonia production rate and ammonia Faradaic efficiency reached 1510.3 μg h^{-1} $mg_{cat.}^{-1}$ and 84.04%, respectively. In these catalysts, the *in-situ* reconstructed Cu^0 serves as the catalytically

* Corresponding author.
E-mail address: zhuyunqing@sust.edu.cn (Y. Zhu).

https://doi.org/10.1016/j.cclet.2024.110399
1001-8417/

active site for NO_3^-RR. Furthermore, the electrochemical reduction potential can drive the generation of defects, leading to significant structural disorder [24,25]. However, the impact of such structural disorder has been seldom explored on NO_3^-RR. The introduction of substantial structural perturbations induces lattice distortion, resulting in the amorphization of materials. Amorphous materials with disordered structures have been widely applied in many electrocatalytic reactions due to their high structural flexibility and exposure of abundant unsaturated active sites [26,27]. Nonetheless, as indicated in previously reported works, structural amorphization often involves complex processing. It typically requires hazardous gas treatment or high-energy ion implantation at elevated temperatures [28,29]. Consequently, constructing a catalyst with a disordered structure through a simple approach for exploring the electrocatalytic nitrate reduction performance at low NO_3^--N concentrations is of vital importance.

In this study, a Cu_3N NRs pre-catalyst with a nanorod structure was synthesized through chemical oxidation and nitrification. Under electrocatalytic nitrate reduction conditions, it underwent *in-situ* reconstruction to form a Cu-based catalyst with a disordered structure of Cu^0 (re-Cu NRs). Structural characterization and electrochemical analysis revealed that the reconstructed Cu^0, acting as the active catalytic species for the conversion of NO_3^--N to NH_4^+-N, exhibited amorphous boundaries that exposed numerous unsaturated active sites. As anticipated, the reconstructed re-Cu NRs material demonstrated excellent catalytic performance of NO_3^-RR and long-term stability at low concentrations of NO_3^--N. The use of ^{15}N labeling confirmed the generation of NH_4^+ during NO_3^-RR. The detection of intermediate products through online differential electrochemical mass spectrometry (DEMS) was employed to infer possible reaction pathways. Density functional theory (DFT) calculations confirmed that the amorphous structure of the re-Cu NRs catalyst facilitated nitrate adsorption and suppression of coexisting hydrogen evolution reactions. Finally, this work combined electrocatalytic NO_3^-RR and electrochlorination through the conversion path of NO_3^--N → NH_4^+-N → N_2, achieving efficient and environmentally benign nitrate treatment.

The synthesis strategy for re-Cu NRs is illustrated in Fig. S1 (Supporting information). Initially, copper foam underwent wet chemical oxidation in a mixed solution of NaOH and $(NH_4)_2S_2O_8$, resulting in vertically aligned $Cu(OH)_2$ nanorods (NRs) arrays. Subsequently, nitrification was performed using urea in a nitrogen atmosphere at 350 °C to form Cu_3N NRs. The prepared Cu_3N NRs was then employed as a pre-catalyst directly for electrochemical nitrate reduction, leading to the *in-situ* reconstruction of re-Cu NRs under electrocatalytic conditions. Morphological characterization of the prepared material was conducted using scanning electron microscopy (SEM). Fig. 1 depicts the surface morphology of $Cu(OH)_2$NRs/CF, Cu_3N NRs, and re-Cu NRs at various magnifications. As shown in Figs. 1a-c, after chemical oxidation, $Cu(OH)_2$ NRs with a length of approximately 5–8 μm and a diameter of about 250 nm uniformly grew on the CF surface. Cu_3N NRs/CF maintained the original morphology after nitrification at 350 °C for 120 min, revealing that each nanorod was composed of stacked nanoparticles (Figs. 1d-f). Figs. 1g-i display the further changes in re-Cu NRs after electrochemical reduction. The reconstructed nanorod surface became rougher, exposing a larger specific surface area, which facilitates enhanced charge transfer and is advantageous for electrocatalytic applications [19].

Further morphological and structural analysis of re-Cu NRs was conducted using transmission electron microscopy (TEM). Fig. 2a illustrates the overall structure of re-Cu NRs, revealing that the nanorods were composed of numerous nanoparticles with sizes around 25-30 nm. High-resolution transmission electron microscopy (HRTEM) provides clear insight into the ordered crystal structure inside the nanoparticles and the amorphous structure at

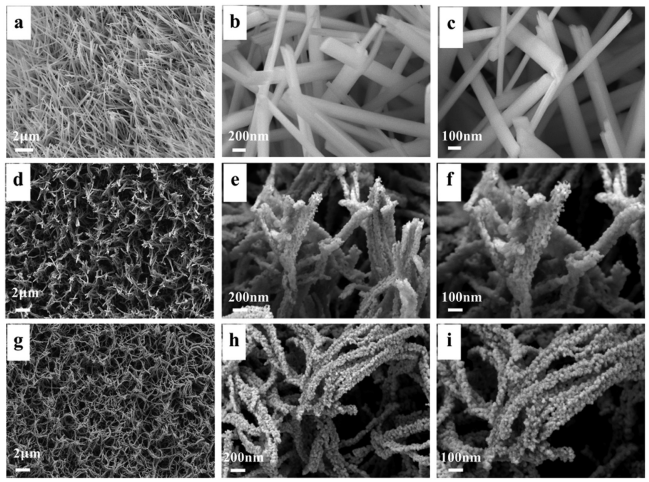

Fig. 1. SEM images of (a-c) $Cu(OH)_2$ NRs/CF, (d-f) Cu_3N NRs, and (g-i) re-Cu NRs at different magnifications.

the interface (marked by the white dashed curve in Fig. 2b. Simultaneously, a clear lattice spacing of 0.210 nm corresponding to the crystal plane (111) of Cu can be observed in the crystalline region. For Cu_3N NRs, the crystal structure of Cu_3N is easily identified with a lattice spacing of 0.382 nm corresponding to the crystal plane (100) of Cu_3N (Fig. S2 in Supporting information) [30]. The transition from the crystal plane (100) of Cu_3N to the crystal plane (111) of Cu confirms the *in-situ* reconstruction of Cu_3N NRs during the electrochemical reduction process. Moreover, it is worth noting that the *in-situ* reconstruction resulted in the amorphous boundary region around the nanoparticles, contributing to enhanced electrocatalytic activity. Compared to crystal structures, the disordered atomic arrangement in amorphous structures exposes abundant active sites with unsaturated structures, favouring the adsorption and conversion of NO_3^--N [31,32]. Subsequent scanning transmission electron microscopy-energy dispersive spectroscopy (STEM-EDS) results (Fig. S3 in Supporting information) also show a decrease in the nitrogen content on the surface of Cu_3N NRs electrodes, validating the *in-situ* transformation from Cu_3N to Cu during the electrochemical reduction process.

To investigate the chemical changes during the *in-situ* reduction of Cu_3N NRAs, X-ray diffraction (XRD) and high-resolution X-ray photoelectron spectroscopy (XPS) tests were conducted. Fig. 2c displays the XRD patterns of Cu_3N NRs and re-Cu NRs. The peaks at 23.3°, 33.2°, 40.9°, 47.6°, 53.6°, and 69.6° corresponded well to the planes (100), (110), (111), (200), (210), and (220) of the cubic structure of Cu_3N (JCPDFS No. 47–1088), consistent with previous reports [30,33]. After electrochemical reduction, the peaks of Cu_3N disappeared, leaving three characteristic peaks at 43.29°, 50.43°, and 74.13°, corresponding to the planes (111), (200), and (220) of the cubic Cu (JCPDS No. 04–0836). This is in accordance with the TEM analysis results.

To further test the surface composition and chemical states of these two samples, XPS analysis was performed. As shown in Fig. 2d, the two peaks cantered at 932.2 eV and 952.0 eV in the Cu 2p spectrum could be assigned to Cu $2p_{3/2}$ and Cu $2p_{1/2}$, respectively. To further distinguish between Cu^+ and Cu^0, the chemical state of copper was identified with auger electron spectroscopy (AES) (Fig. 2e). There is only one characteristic peak centered on 917.1 eV from Cu^+ in the Cu_3N NRs [34,35]. After electrochemical reduction, a new peak cantered at 918.8 eV appeared on the surface of re-Cu NRs, corresponding to Cu^0, indicating the conversion of Cu^+ to Cu^0 occurring during the reconstruction process [18,23]. It is noteworthy that the Cu 2p XPS spectrum of re-Cu NRs exhibited a negative shift compared to Cu_3N NRs (Fig. 2d). In contrast, the Cu^0 Auger

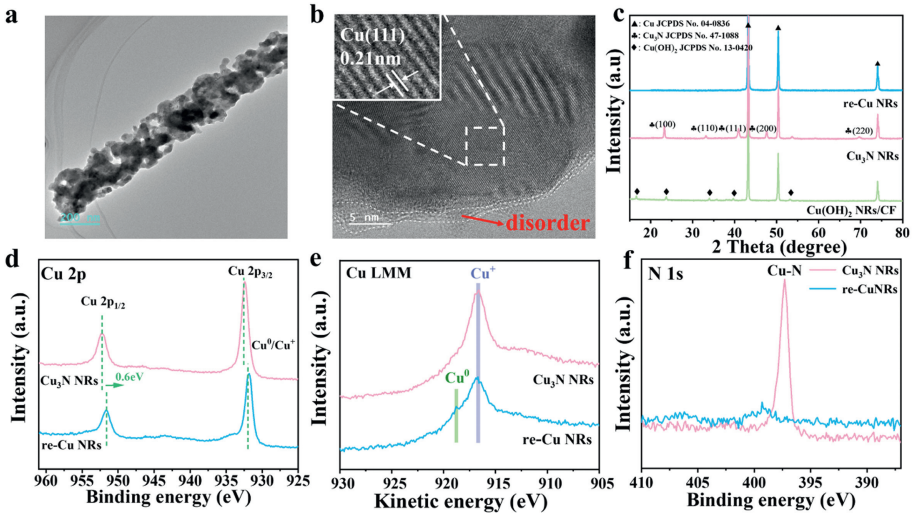

Fig. 2. (a) TEM and (b) HRTEM images of re-Cu NRs. (c) XRD patterns of $Cu(OH)_2$ NRs/CF, Cu_3N NRs, and re-Cu NRs electrodes. (d) Cu 2p XPS spectra, (e) Cu LMM AES spectra, and (f) N 1s XPS spectra of Cu_3N NRs and re-Cu NRs electrodes.

peak in the re-Cu NRs electrode had a positive shift of 0.2 eV compared to pure Cu metal (918.6 eV), indicating the presence of electron transfer at the re-Cu NRs electrode interface [19]. Simultaneously, in the N 1s spectrum (Fig. 2f), the peak corresponding to the Cu-N bond at a binding energy of 397.3 eV disappeared [30,36]. The above results indicate that the re-Cu NRs with amorphous boundaries are the active substances during electrocatalytic nitrate reduction.

In a single-chamber electrolytic cell, the electrocatalytic performance of the re-Cu NRs electrode was evaluated using Ag/AgCl and Pt foil as reference electrode and counter electrode, respectively. Linear sweep voltammetry (LSV) polarization curves for different electrodes in a 50 mg/L NO_3^--N and 0.05 mol/L Na_2SO_4 solution are shown in Fig. 3a. Compared to CF substrate and $Cu(OH)_2$ NRs/CF electrode, the re-Cu NRs electrode exhibited higher current density, indicating superior electrocatalytic nitrate reduction performance. The double-layer capacitance (C_{dl}) values of re-Cu NRs were calculated from the cyclic voltammetry (CV) curves at different scan rates (1–5 mV/s) (Fig. S4 in Supporting information). As shown in Fig. 3b, the C_{dl} value of re-Cu NRs was 123.12 mF/cm^2, which was 1.54 times that of $Cu(OH)_2$ NRs/CF (79.9 mF/cm^2), and 19.05 times that of CF substrate (6.46 mF/cm^2). The larger electrochemical active surface area of re-Cu NRs may be attributed to the amorphous boundaries formed by structural disorder, exposing more abundant active sites [37]. Furthermore, electrochemical impedance spectroscopy (EIS) measurements were conducted to study the electron transfer rate of the prepared re-Cu NRs electrode (Fig. 3c). The Nyquist plot for re-Cu NRs exhibited a smaller arc diameter compared to $Cu(OH)_2$ NRs/CF electrode and CF substrate, demonstrating that the charge transfer resistance of re-Cu NRs was minimal. This suggests fast electron transfer rates during the electrochemical reaction, contributing to superior reaction kinetics and enhanced catalytic activity for NO_3^-RR [38,39].

To further explore the electrocatalytic performance of re-Cu NRs, electrocatalytic NO_3^-RR experiments were conducted at different applied potentials ranging from −0.9 V to −1.4 V. The concentrations of reactants and reduction products (NO_3^--N, NO_2^--N, and NH_4^+-N) were detected using spectrophotometry, and corresponding concentration-absorbance calibration curves were plotted (Fig. S5 in Supporting information). As shown in Fig. 3d, with the increase in applied potential, the conversion rate of NO_3^--N continually increased, reaching 100% at −1.2 V and gradually stabilizing. Additionally, the electrocatalytic nitrate reduction process at different applied potentials conformed to the *pseudo*-first-order kinetic model (Fig. S6 in Supporting information). With the increase in working potential, the reduction rate of NO_3^--N and the corresponding *pseudo*-first-order kinetic constant (k) gradually increased (from 0.01063 min^{-1} to 0.05231 min^{-1}). As the applied potential increased from −0.9 V to −1.4 V, the NH_4^+-N selectivity gradually increased, reaching 99.60% at −1.2 V, while the NO_2^--N selectivity gradually decreased (Fig. S7 in Supporting information). As seen in Fig. 3e, the yield and Faradaic efficiency of NH_3 at different applied potentials exhibited a volcano-shaped curve, reaching peak values of 238.87 μg h^{-1} cm^{-2} and 44.30% at −1.2 V, respectively. This might be attributed to the intensified HER with the increase in applied potential, leading to a decrease in Faradaic efficiency [14]. Therefore, −1.2 V was identified as the most suitable applied potential for the electrocatalytic reduction of nitrate by re-Cu NRs.

Considering the practical application of re-Cu NRs in real wastewater, the impact of different initial concentrations of nitrate on electrocatalytic NO_3^-RR was investigated. As shown in Fig. 3f, with the initial nitrate concentration increasing from 25 mg/L to 150 mg/L, the conversion rate of NO_3^--N decreased from 100% to 72.8%. This is possibly due to the limited active sites on the electrode surface, where excess NO_3^--N might not fully contact the electrode, restricting its adsorption on the active sites [40]. In addition, with the increase in initial NO_3^--N concentration, the selectivity of NH_4^+-N gradually decreased, and the yield of NH_3 decreased from 238.87 μg h^{-1} cm^{-2} and stabilized at 165.23 μg h^{-1} cm^{-2}. This phenomenon suggests that excessively high concentrations of NO_3^--N are unfavourable for NH_4^+-N production. This could be attributed to the competition between NO_3^--N and NO_2^--N for reaction centres, where some NO_2^--N was displaced from the reaction centres before being hydrogenated to form NH_4^+-N [41]. The re-Cu NRs exhibited higher nitrate conversion rates and ammonia yields at low concentrations, which could be directly applied to the *in-situ* remediation of water bodies with low-concentration nitrate pollution.

To explore the source of ammonia in electrochemical NO_3^-RR and eliminate the interference of the external environment on the experimental results, several comparative experiments were carried out. In the comparative experiments conducted in a solution containing only Na_2SO_4, no ammonia generation was detected, proving that ammonia did not originate from the elec-

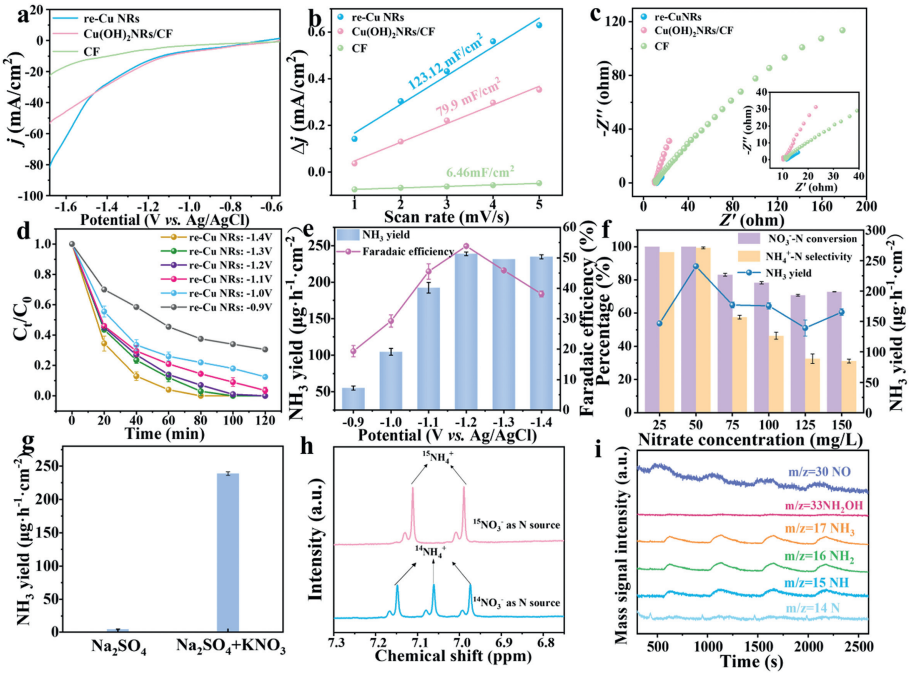

Fig. 3. (a) LSV curves of CF, $Cu(OH)_2$ NRs/CF, and re-Cu NRs in 0.05 mol/L Na_2SO_4 electrolyte with 50 mg/L NO_3^--N. (b) Normalised electrochemical active surface area (ECSA) current densities and (c) Nyquist plots of catalysts. (d) The nitrate removal rate of re-Cu NRs at different application potentials. (e) Potential-dependent Faradaic efficiency and yield rate of NH_4^+ over re-Cu NRs. (f) NO_3^--N conversion, NH_4^+-N selectivity, and NH_3 yield rate with re-Cu NRs under different nitrate concentrations. (g) NH_3 yield rates of the re-Cu NRs in 0.05 mol/L Na_2SO_4 with and without 50 mg/L NO_3^--N. (h) ^1H NMR spectra of the electrolyte after the electrocatalytic reaction using $^{15}NO_3^-$ and $^{14}NO_3^-$ as the nitrogen sources. (i) DEMS measurements of the NO_3^-RR on re-Cu NRs (four cycles under the potential of −1.2 V).

trocatalyst (Fig. 3g). To further identify the source of ammonia, the isotope labelling experiment was conducted. As shown in the ^1H NMR spectrum (Fig. 3h) using $K^{14}NO_3$ and $K^{15}NO_3$ as reactants for the electrolytic reaction, the detected $^{14}NH_4^+$–^{14}N exhibited a typical triple-peak pattern, while $^{15}NH_4^+$–^{15}N showed a characteristic double-peak pattern [16,23]. This result affirmed that the generation of NH_4^+ indeed originated from electrochemical NO_3^-RR. Additionally, maleic acid ($C_4H_4O_4$) was used as an internal standard to quantify the generated NH_4^+-N based on the standard curve of the integration area *versus* NH_4^+ concentration (NH_4^+-N/$C_4H_4O_4$) (Fig. S8 in Supporting information). The results revealed that the concentrations of $^{15}NH_4^+$–^{15}N (48.89 mg/L) and $^{14}NH_4^+$–^{14}N (49.02 mg/L) produced after 120 min of electrocatalytic nitrate reduction were very close to the determined concentrations by UV–vis spectrophotometry, confirming the accuracy of this method.

To elucidate the reaction pathways of the electrocatalytic process, online DEMS was employed to detect intermediates and products generated at the re-Cu NRs cathode during the electrocatalytic NO_3^-RR process. Fig. 3i displays the *m/z* signals detected by online DEMS at an applied potential of −1.2 V, corresponding to species NO, NH, NH_2, and NH_3 with *m/z* values of 30, 15, 16, and 17, respectively. Moreover, no signal of NHOH (*m/z* = 32) was observed in the DEMS detection results, allowing us to propose the NO_3^-RR reaction pathway on the surface of re-Cu NRs and used for theoretical calculations.

DFT calculations have been further conducted to demonstrate the significant contribution of the amorphous structure of the re-Cu NRs catalysts to the NO_3^-RR. The schematic diagram of the process from Cu_3N NRs to re-Cu NRs is shown in Fig. 4a. In this process, the Cu_3N precatalyst suffers from the N leaching phenomenon, in which the N atoms are detached from the Cu_3N structure into the solution to form NH_4^+-N (Fig. S9 in Supporting information), and finally, the Cu_3N NRs is reconfigured as re-Cu NRs

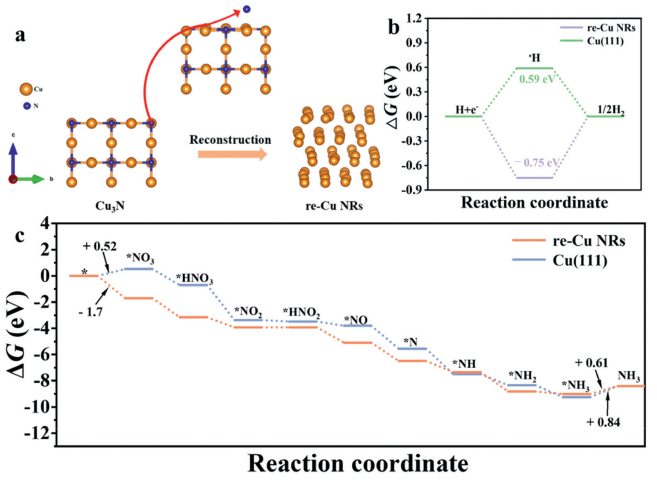

Fig. 4. (a) Schematic of the reconstruction process to re-Cu NRs from Cu_3N NRs. (b) Gibbs free energy diagram of HER. (c) Reaction energy diagrams of the NO_3^-RR pathway on the surface of re-Cu NRs and Cu (111).

with an amorphous structure. A computational model of re-Cu NRs with an amorphous structure was simulated with DFT, and Cu (111) was selected as the theoretical computational model of the Cu samples for comparison, considering the lattice spacing of the Cu (111) facet shown in the TEM. The primary competitive reaction for the electrocatalytic nitrate reduction reaction was HER, so the energies of the hydrogen evolution reactions were determined. As shown in Fig. 4b, the Gibbs free energy for the formation of H_2 on re-Cu NRs was 0.75 eV, which was above the energy required for Cu (111) (0.59 eV), indicating that re-Cu NRs had an inhibition effect on H_2 generation [42]. Moreover, based on the DEMS de-

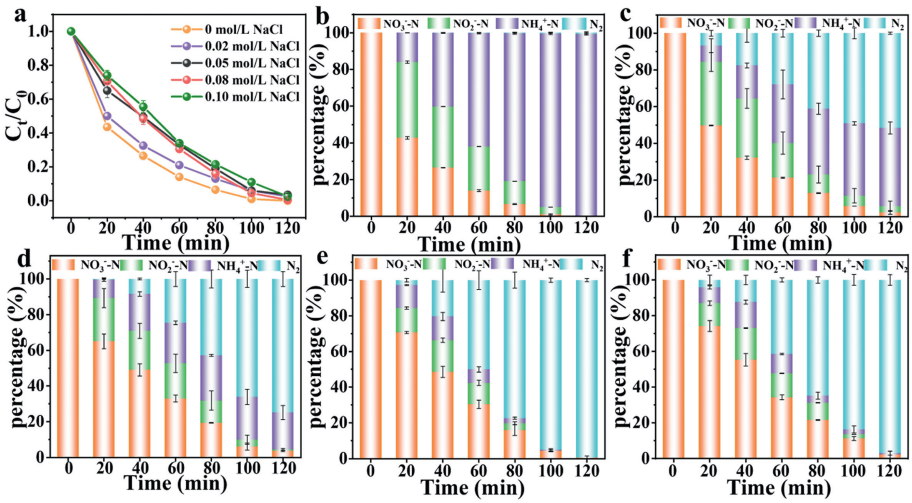

Fig. 5. (a) Effect of NaCl concentration on NO_3^--N removal. Selectivity-time curves for inorganic-N product (b) in the absence of NaCl, (c) with 0.02 mol/L NaCl, (d) with 0.05 mol/L NaCl, (e) with 0.08 mol/L NaCl, and (f) with 0.10 mol/L NaCl. Experimental conditions: 50 mol/L NO_3^--N, 0.05 mol/L Na_2SO_4, −1.2 V of applied potential, and 120 min treatment.

rived NO_3^-RR reaction pathway on the surface of re-Cu NRs, the free energies of all the reduction intermediates on the surface of re-Cu NRs and Cu (111) were calculated (Fig. 4c). The model of the most stable adsorption of all intermediates on re-Cu NRs and Cu (111) surfaces is shown in Fig. S10 (Supporting information). During the process, NO_3^- was initially adsorbed on the catalyst surface, forming adsorbed nitrate ($*NO_3^-$). As can be seen in Fig. 4c, the free energy of NO_3^- to form $*NO_3^-$ on the Cu (111) surface was 0.52 eV, much higher than that of the re-Cu NRs (−1.70 eV), suggesting that the amorphous structure could promote the adsorption of NO_3^- on the surface of the catalyst and accelerate the subsequent reaction. Then, the N–O bond is continuously cleaved by proton-coupled electron transfer to form $*NO_2$ and *NO. Thereafter, the *NO intermediates were gradually converted to *N, *NH, $*NH_2$, and finally $*NH_3$ under hydrogenation [18]. It is noteworthy that the desorption of NH_3 from the catalyst surface is a potential determining step in the overall nitrate reduction process. The energy barrier of 0.61 eV is required at the re-Cu NRs for the formation of NH_3, lower than that at the Cu (111) surface (0.84 eV), indicating that the desorption of $*NH_3$ more easily proceeds at the surface of re-Cu NRs with an amorphous structure [43]. Therefore, DFT calculations of NO_3^-RR and HER simulations showed that re-Cu NRs with an amorphous boundary not only enhanced NO_3^- adsorption but also optimized the adsorption energy of the intermediates ($*NH_3 \rightarrow NH_3$) and inhibited the formation of H_2, leading to enhanced intrinsic electrocatalytic NO_3^-RR activity.

To achieve complete conversion of NO_3^--N to harmless N_2, electrochemical NO_3^-RR experiments were conducted in the presence of Cl^-. Breakpoint chlorination is a widely used method for drinking water treatment, where the anodic *in-situ* oxidation of Cl^- generates active chlorine species ($HOCl/ClO^-$), facilitating the conversion of NH_4^+-N to N_2 [44,45]. Therefore, we selectively investigated the effect of NaCl concentration on NO_3^--N conversion, NO_2^--N generation, NH_4^+-N generation and N_2 generation in the three-electrode device with Ag/AgCl and Pt foil as the reference and counter electrodes, respectively, and re-Cu NRs as working electrode. As shown in Fig. 5a, in the electrolyte without NaCl, the removal efficiency of NO_3^--N reached 100%, and it was not affected by the increase in NaCl concentration. As can be seen in Fig. 5b, the NO_2^--N production reached a maximum value of 20.09 mg/L with 20 min in the absence of NaCl, it decreased over time and eventually failed to be detectable. Meanwhile, the selectivity of NH_4^+-N continuously increased, reaching

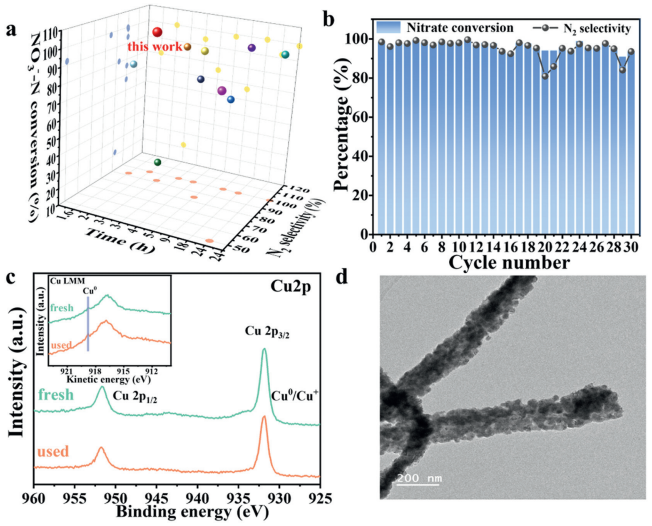

Fig. 6. (a) Summary of the N_2 selectivity and NO_3^- conversion in electrocatalytic NO_3^-RR process with Cu-based electrocatalysts reported in the literature. (b) Stability tests of the re-Cu NRs electrode towards nitrate conversion and N_2 selectivity in Na_2SO_4−NaCl electrolytes (2 h treatment of each cycle). (c) XPS Cu 2p spectra and Cu LMM spectra (inset) of fresh and used re-Cu NRs electrodes. (d) TEM images of re-Cu NRs after stability tests for electrocatalytic NO_3^-RR.

98.94% at 120 min. The product distribution of the re-Cu NRs electrode in NaCl electrolyte during the electrocatalytic nitrate reduction process was further analysed to elucidate the influence of NaCl (Figs. 5c-e). With the rise in NaCl concentration, the generation of NH_4^+-N and NO_2^--N was significantly suppressed. When the NaCl concentration was 0.02, 0.05, and 0.08 mol/L, the selectivity for N_2 was 51.66%, 74.88%, and 99.41%, respectively. After electrolysis in a solution containing 0.08 mol/L NaCl for 120 min, no residual NO_2^--N was detected. It is noteworthy that further increasing the sodium chloride concentration to 0.10 mol/L did not further improve the selectivity for N_2 (Fig. 5f). Therefore, re-Cu NRs electrodes combined with anodic chlorine oxidation could effectively remove NO_3^--N and NO_2^--N and simultaneously convert NH_4^+-N to harmless N_2 in an electrolyte containing 0.08 mol/L NaCl.

Table S1 (Supportting information) and Fig. 6a summarize and compare the removal efficiency for NO_3^--N and N_2 selectivity of Cu-based catalysts as reported in recent studies. Through the de-

signed pathway combined with electrochlorination, the re-Cu NRs cathode achieved higher NO_3^--N removal efficiency and N_2 selectivity in a short time compared with other catalytic materials. The enhanced electrocatalytic NO_3^-RR activity of re-Cu NRs could be mainly attributed to the *in-situ* reconstruction of Cu_3N NRs. During the *in-situ* electrochemical reduction process, Cu_3N NRs could transform into re-Cu NRs with amorphous boundaries, where Cu^0 species acted as active sites to enhance NO_3^-RR performance. Furthermore, *in-situ* reconstruction resulted in the formation of amorphous boundaries around nanoparticles with more defects and catalytic sites, thereby facilitating the adsorption, dissociation, and conversion of electrocatalytic intermediates [26,31,32].

Transition metal electrodes are prone to corrosion during electrolysis, leading to leaching of metal ions and secondary metal contamination. This is the reason why the stability of electrocatalysts is crucial in practical applications. To assess the stability of re-Cu NRs, cyclic experiments were conducted under optimal conditions. As shown in Fig. 6b, during 30 cycles of electrocatalytic nitrate reduction in Na_2SO_4–NaCl electrolyte, the re-Cu NRs cathode exhibited high catalytic stability, maintaining a conversion rate of nitrate between 90%−100%, and an average N_2 selectivity above 90%. The inductively coupled plasma mass spectrometry (ICP-MS) results demonstrated a low leaching of copper ions in the electrolyte after the reaction (Fig. S11 in Supporting information). Moreover, the Cu 2p profiles of fresh and used re-Cu NRs catalysts exhibited Cu $2p_{3/2}$ and Cu $2p_{1/2}$ peaks at 932.2 eV and 952.0 eV, respectively, and the Cu^0 peak was still clearly visualized in the Cu LMM profile (Fig. 6c and its inset). It indicates that the Cu^0 formation by *in-situ* reconfiguration could exist stably during electrocatalytic reduction, which is verified to have good stability. TEM characterization of the re-Cu NRs after the electrocatalytic reaction revealed that the re-Cu NRs still maintained its original nanorod morphology, demonstrating that the structure of the material has not changed after cycling (Fig. 6d). These findings indicate that the re-Cu NRs catalyst, with amorphous boundaries formed after reconstruction, exhibited excellent stability in multiple cycles.

In summary, a re-Cu NRs catalyst with an amorphous structure was prepared through *in-situ* electrochemical reconstruction. The well-defined three-dimensional nanorods structure and the amorphous boundaries on the surface expose abundant active sites, improving the performance of adsorption and conversion of NO_3^--N at low concentrations. The results of electrocatalytic NO_3^-RR indicated that the re-Cu NRs electrode reached 100% NO_3^--N conversion with a superior ammonia selectivity of 99.60% at −1.2 V. Simultaneously, with the assistance of electrochlorination, the electrocatalytic system efficiently converts NH_4^+-N to N_2, achieving a final selectivity of 99.41%. The on-line DEMS was carried out to capture the intermediates for inferring the reaction pathway of NO_3^-RR, and DFT calculations were performed based on the pathway. It is found that re-Cu NRs with amorphous boundaries modulate the adsorption energy of reactants/intermediates and effectively inhibit the occurrence of HER, leading to excellent electrocatalytic activity and selectivity. This work proves that the amorphous Cu-based catalysts prepared with electrochemical *in-situ* reconfiguration exhibit high efficiency and stability in electrocatalytic NO_3^-RR performance.

Declaration of competing interest

The authors declare that they have no known competing financial interests or personal relationships that could have appeared to influence the work reported in this paper.

CRediT authorship contribution statement

Yunqing Zhu: Conceptualization, Methodology, Writing – review & editing, Supervision, Project administration, Funding acquisition, Resources, Validation. **Kaiyue Wen:** Data curation, Conceptualization, Methodology, Validation, Investigation, Writing – original draft. **Xuequan Wan:** Methodology, Validation, Investigation. **Gaigai Dong:** Supervision, Validation, Visualization. **Junfeng Niu:** Supervision, Formal analysis, Methodology, Supervision, Resources.

Acknowledgments

This work was financially supported by the National Natural Science Foundation of China (No. 21876105), Shaanxi "Scientist & Engineer" Team (No. 2023KXJ-131) and Xianyang Key S&T Special Projects (No. L2023-ZDKJ-QCY-SXGG-GY-007). The authors would like to thank Shiyanjia Lab (www.shiyanjia.com) for supporting SEM and XPS tests.

Supplementary materials

Supplementary material associated with this article can be found, in the online version, at doi:10.1016/j.cclet.2024.110399.

References

[1] X. Zhang, Y. Zhang, P. Shi, et al., Sci. Total Environ. 770 (2021) 144674.
[2] S. Singh, A.G. Anil, V. Kumar, et al., Chemosphere 187 (2022) 131996.
[3] X. Zou, C. Chen, C. Wang, et al., Sci. Total Environ. 800 (2021) 149645.
[4] X. Zhang, Y. Wang, C. Liu, et al., Chem. Eng. J. 403 (2021) 126269.
[5] J. Chen, M. Gu, Y. Zhou, et al., Chem. Eng. J. 430 (2022) 132952.
[6] M. Kalaruban, P. Loganathan, W.G. Shim, et al., Sep. Purif. Technol. 158 (2016) 62–70.
[7] W. Li, S. Patton, J.M. Gleason, et al., Environ. Sci. Technol. 52 (2018) 6417–6425.
[8] L. Gao, F. Han, X. Zhang, et al., Bioresour. Technol. 314 (2020) 123714.
[9] R. Chauhan, V.C. Srivastava, Chem. Eng. J. 386 (2020) 122065.
[10] S. Meng, Y. Ling, M. Yang, et al., J. Environ. Chem. Eng. 11 (2023) 109418.
[11] F. Pan, J. Zhou, T. Wang, et al., J. Colloid Interf. Sci. 638 (2023) 26–38.
[12] Y. Wang, C. Wang, M. Li, et al., Chem. Soc. Rev. 50 (2021) 6720–6733.
[13] F.Y. Chen, Z.Y. Wu, S. Gupta, et al., Nat. Nanotechnol. 17 (2022) 759–767.
[14] Y. Xue, Q. Yu, J. Fang, et al., Small 20 (2024) 2400505.
[15] F. Ni, Y. Ma, J. Chen, et al., Chin. Chem. Lett. 32 (2021) 2073–2078.
[16] W. Zheng, L. Zhu, Z. Yan, et al., Environ. Sci. Technol. 55 (2021) 13231–13243.
[17] G. Tokazhanov, E. Ramazanova, S. Hamid, et al., Chem. Eng. J. 384 (2020) 12352.
[18] Y. Wang, W. Zhou, R. Jia, et al., Angew. Chem. Int. Ed. 59 (2020) 5350–5354.
[19] J. Zhou, F. Pan, Q. Yao, et al., Appl. Catal. B: Environ. 317 (2022) 121811.
[20] Y. Wang, A. Xu, Z. Wang, et al., J. Am. Chem. Soc. 142 (2020) 5702–5708.
[21] J. Cai, Y. Wei, A. Cao, et al., Appl. Catal. B: Environ. 316 (2022) 121683.
[22] Q. Song, S. Zhang, X. Hou, et al., J. Hazard. Mater. 438 (2022) 129455.
[23] H. Yu, K. Deng, Z. Wang, et al., Appl. Catal. B: Environ. 318 (2022) 121805.
[24] P.L. Gai-Boyes, Catal. Rev. 34 (1992) 1–54.
[25] S. Sun, T. Zhai, C. Liang, et al., Nano Energy 45 (2018) 390–397.
[26] L. Zhang, H. Jang, H. Liu, et al., Angew. Chem. Int. Ed. 60 (2021) 18821–18829.
[27] S. Deng, Z. Yuan, Z. Tie, et al., Angew. Chem. Int. Ed. 59 (2020) 22002–22006.
[28] N. Liu, V. Häublein, X. Zhou, et al., Nano Lett. 15 (2015) 6815–6820.
[29] L. Li, Z. Hu, L. Tao, et al., ACS Appl. Energy Mater. 3 (2020) 3071–3081.
[30] P.A. Shinde, S. Park, N.R. Chodankar, et al., Appl. Mater. Today 22 (2021) 100951.
[31] Q. Liang, L. Zhong, C. Du, et al., Adv. Funct. Mater. 2 (2018) 1805075.
[32] X. Wang, X. Yu, S. Wu, et al., ACS Appl. Mater. Interfaces 15 (2023) 15533–15544.
[33] Y. Mi, S. Shen, X. Peng, et al., ChemElectroChem 6 (2019) 2393–2397.
[34] C. Li, S. Liu, Y. Xu, et al., Nanoscale 14 (2022) 12332.
[35] T. Feng, J. Wang, Y. Wang, et al., Chem. Eng. J. 433 (2022) 133495.
[36] Z. Wang, L. Xu, F. Huang, et al., Adv. Energy Mater. 9 (2019) 1900390.
[37] Y. Sun, S. Gao, F. Lei, et al., Chem. Soc. Rev. 44 (2015) 623–636.
[38] H. Xu, J. Wu, W. Luo, et al., Small 16 (2020) 2001775.
[39] M. Fu, Y. Mao, H. Wang, et al., Chin. Chem. Lett. 35 (2024) 108341.
[40] Q. Song, M. Li, X. Hou, et al., Appl. Catal. B: Environ. 317 (2022) 121721.
[41] M. Tang, Q. Tong, Y. Li, et al., Chin. Chem. Lett. 34 (2023) 108410.
[42] J. Zhao, Z. Shen, J. Yu, et al., J. Hazard. Mater. 439 (2022) 129653.
[43] R. Qi, Z. Wang, M. Zhong, et al., Small 20 (2024) 2308311.
[44] M. Li, C. Feng, Z. Zhang, et al., J. Hazard. Mater. 171 (2009) 724–730.
[45] X. Zhang, W. Li, E.R. Blatchley, et al., Water Res. 68 (2015) 804–811.